Hyperdensity Functional Theory of Soft Matter

Florian Sammüller, Silas Robitschko, Sophie Hermann, and Matthias Schmidt

Theoretische Physik II, Physikalisches Institut, Universität Bayreuth, D-95447 Bayreuth, Germany

We present a scheme for investigating arbitrary thermal observables in spatially inhomogeneous equilibrium many-body systems. Extending the grand canonical ensemble yields any given observable as an explicit hyperdensity functional. Associated local fluctuation profiles follow from an exact hyper-Ornstein-Zernike equation. While the local compressibility and simple observables permit analytic treatment, complex order parameters are accessible via simulation-based supervised machine learning of neural hyperdirect correlation functionals. We exemplify efficient and accurate neural predictions for the cluster statistics of hard rods, square-well rods, and hard spheres. The theory allows one to treat complex observables, as is impossible in standard density functional theory.

Classical density functional theory is a powerful framework for describing the collective behavior of a wide variety of relevant many-body systems [1–5]. Topical applications to soft matter [6] range from studies of hydrophobicity [7–11] to investigations of the molecular structure of liquids [11–13] and of electrolytes [14–16]. The central variable of density functional theory is the position-resolved one-body density profile. In recent developments, the local compressibility [8,9,17] and more general fluctuation profiles [18–20] were shown to be further useful indicators for collective phenomena, e.g., when systematically analyzing drying that occurs near substrates and around solutes [8,9,17,20]. A further broad spectrum of observables, including recent multibody correlation functions [21–23], are relevant for the study of complex systems.

The use of statistical mechanical sum rules [1,4,24,25] is often decisive in the description of soft matter, as sum rules not only provide unambiguous consistency checks, but also as they encapsulate physical constraints, which ultimately facilitates to trace physical mechanisms and identify underlying causes for the emerging collective effects. In line with further topical uses of the Noether theorem in statistical mechanics [26–32], the recent thermal Noether invariance theory [33–35] allows one to systematically generate and classify a significant body of exact sum rules. The properties of general observables can be addressed via the recent hyperforce theory [35], which is similar in spirit to Hirschfelder's hypervirial generalization [36] of the standard virial theorem [4].

Machine learning techniques see a rapidly increasing use in soft matter research across topics that range from characterization [37] to engineering of self-assembly [38], detection of colloidal structure [39], and the study of effective colloidal interaction potentials [40,41]. In the context of density functional theory, machine learning was used for the construction of workable representations for the central functional both in the classical [42–55] and in the quantum realms [55–63]. The recent neural functional theory [50–52] constitutes a hybrid method that is based on many-body computer simulation data used to train a neural network, which then acts as a central numerical object that mirrors the functional structure prescribed by classical density functional theory.

Here we return to fundamentals and present a generalization of classical density functional theory that allows one to investigate the behavior of virtually arbitrary observables and their locally resolved fluctuation profiles. We specifically develop a general variational formalism based on an extended thermal ensemble [64,65]. While the theory is formally exact, we demonstrate as one way forward that the relevant functional dependencies are amenable to supervised machine learning. We present model demonstrations for what we argue is a stand-alone and practically relevant computational scheme for the investigation of soft matter. Our approach rests on the Mermin-Evans functional map [1,66], which ascertains that any equilibrium quantity can be expressed as a density functional.

Density functional theory [1,4] puts the one-body density distribution,

$$\rho(\mathbf{r}) = \langle \hat{\rho}(\mathbf{r}) \rangle, \tag{1}$$

at center stage. Here we have defined the one-body density "operator" in its standard form $\hat{\rho}(\mathbf{r}) = \sum_i \delta(\mathbf{r} - \mathbf{r}_i)$, with $\delta(\cdot)$ denoting the Dirac distribution, $\mathbf{r}$ is a generic position variable, $\mathbf{r}_i$ is the position of particle $i = 1, \ldots, N$, and $\langle \cdot \rangle$ indicates the thermal average as specified below in detail. In the following we consider a general observable that is represented by a phase space function $\hat{A}(\mathbf{r}^N)$, which in general depends on the position coordinates $\mathbf{r}^N$ of all

N particles, as well as possibly on additional parameters. Following its occurrence in the hyperforce theory [35], in generalization of the one-body fluctuation profiles of Refs. [8,9,18–20], and borrowing the terminology from the hypervirial theorem [36], we consider a corresponding hyperfluctuation profile $\chi_A(\mathbf{r})$ as the covariance of the density operator and the given observable. Together with the mean A we hence define

$$A = \langle \hat{A} \rangle, \tag{2}$$

$$\chi_A(\mathbf{r}) = \mathrm{cov}(\hat{\rho}(\mathbf{r}), \hat{A}), \tag{3}$$

with the standard covariance $\mathrm{cov}(\hat{X}, \hat{Y}) = \langle \hat{X}\hat{Y} \rangle - \langle \hat{X} \rangle \langle \hat{Y} \rangle$ of two phase space functions $\hat{X}$ and $\hat{Y}$.

Specifically, we consider classical many-body systems of N particles of identical mass m. The Hamiltonian has the standard form $H = \sum_i \mathbf{p}_i^2/(2m) + u(\mathbf{r}^N) + \sum_i V_{\mathrm{ext}}(\mathbf{r}_i)$, where the sums run over all particles $i = 1, \ldots, N$, the momentum of particle i is denoted by $\mathbf{p}_i$, the interparticle interaction potential is $u(\mathbf{r}^N)$, where $\mathbf{r}^N \equiv \mathbf{r}_1, \ldots, \mathbf{r}_N$ is a shorthand for all position coordinates, and $V_{\mathrm{ext}}(\mathbf{r})$ is an external potential, here written as a function of the (generic) position coordinate $\mathbf{r}$. We work in the grand ensemble at absolute temperature T and chemical potential μ. The classical "trace" operation is defined as $\mathrm{Tr} \cdot = \sum_{N=0}^{\infty} (h^{dN} N!)^{-1} \int d\mathbf{r}^N d\mathbf{p}^N \cdot$, where h denotes the Planck constant, d the spatial dimensionality, and $\int d\mathbf{r}^N d\mathbf{p}^N$ indicates the phase space integral over all position coordinates and momenta.

To incorporate the observable $\hat{A}(\mathbf{r}^N)$ into the framework, we consider an extended ensemble [64,65] that is here defined by the extended equilibrium many-body probability distribution $\mathrm{e}^{-\beta(H-\mu N)+\lambda\hat{A}}/\Xi$, where λ is a coupling parameter that acts as a conjugate variable to $\hat{A}(\mathbf{r}^N)$; here $\beta = 1/(k_B T)$ with k_B denoting the Boltzmann constant. The extended grand partition sum is given as $\Xi = \mathrm{Tr}\, \mathrm{e}^{-\beta(H-\mu N)+\lambda\hat{A}}$ and the corresponding grand potential is $\Omega = -k_B T \ln \Xi$. Thermal averages are obtained via $\langle \cdot \rangle = \mathrm{Tr} \cdot \mathrm{e}^{-\beta(H-\mu N)+\lambda\hat{A}}/\Xi$. An alternative and equivalent view of the extended ensemble can be based on rather considering an extended Hamiltonian $H_A = H - \lambda\hat{A}/\beta$ and formulating its associated standard grand ensemble.

Despite the generalization, we remain only interested in the properties of the original system with Hamiltonian H, recovering its standard grand ensemble for the case of vanishing coupling constant, $\lambda \to 0$. Throughout, we assume that $\hat{A}(\mathbf{r}^N)$ is of a form such that the statistical ensemble generated via H_A is well defined in this limit and that indeed $H_A \to H$ recovers the original Hamiltonian (which specifies our above restriction to "virtually" arbitrary observables $\hat{A}$).

The thermal average A and the hyperfluctuation profile $\chi_A(\mathbf{r})$, as respectively defined via Eqs. (2) and (3), are generated via the following partial derivatives with respect to the coupling parameter λ:

$$A = -\frac{\partial \beta \Omega}{\partial \lambda}, \tag{4}$$

$$\chi_A(\mathbf{r}) = \frac{\partial \rho(\mathbf{r})}{\partial \lambda}. \tag{5}$$

The state point μ, T and the form of the external potential $V_{\mathrm{ext}}(\mathbf{r})$ are thereby fixed upon differentiating. That Eqs. (4) and (5) hold can, respectively, be verified by elementary calculations taking into account that $-\beta\Omega = \ln \Xi$ and the definition (1) of $\rho(\mathbf{r})$. Equation (5) is also rapidly derived from the standard expression [1,4] of the density profile as a functional derivative, $\delta\Omega/\delta V_{\mathrm{ext}}(\mathbf{r}) = \rho(\mathbf{r})$, together with Eq. (3) and the recent [19] general identity $-\delta A/\delta\beta V_{\mathrm{ext}}(\mathbf{r}) = \mathrm{cov}(\hat{\rho}(\mathbf{r}), \hat{A}) = \chi_A(\mathbf{r})$. The latter relation is also straightforward to show by explicit calculation and it lends much physical meaning to $\chi_A(\mathbf{r})$ as the response function of the average A against changes in the shape of the scaled external potential $-\beta V_{\mathrm{ext}}(\mathbf{r})$.

The Euler-Lagrange equation of classical density functional theory [1–4], applied to the extended Hamiltonian H_A, has the standard form

$$c_1(\mathbf{r}, [\rho]) = \ln \rho(\mathbf{r}) + \beta V_{\mathrm{ext}}(\mathbf{r}) - \beta\mu, \tag{6}$$

where $c_1(\mathbf{r}, [\rho])$ is the one-body direct correlation functional corresponding to H_A, i.e., for a system of particles that interact via the extended interparticle interaction potential $u(\mathbf{r}^N) - \lambda\hat{A}(\mathbf{r}^N)/\beta$. In Eq. (6) we have set the thermal de Broglie wavelength to unity and we denote functional dependence by square brackets throughout. As Eq. (6) holds for any value of λ, provided that $\rho(\mathbf{r})$ is the corresponding equilibrium density profile, we can differentiate the equation with respect to λ and retain a valid identity. The result is the following hyper-Ornstein-Zernike relation:

$$c_A(\mathbf{r}, [\rho]) = \frac{\chi_A(\mathbf{r})}{\rho(\mathbf{r})} - \int d\mathbf{r}'\, c_2(\mathbf{r}, \mathbf{r}', [\rho])\chi_A(\mathbf{r}'), \tag{7}$$

where $c_2(\mathbf{r}, \mathbf{r}', [\rho]) = \delta c_1(\mathbf{r}, [\rho])/\delta\rho(\mathbf{r}')$ is the two-body direct correlation functional [1–4]. The left-hand side of Eq. (7) constitutes the hyperdirect correlation functional $c_A(\mathbf{r}, [\rho])$, as is obtained from parametrically differentiating the left-hand side of Eq. (6) at fixed density profile,

$$c_A(\mathbf{r}, [\rho]) = \left. \frac{\partial c_1(\mathbf{r}, [\rho])}{\partial \lambda} \right|_\rho. \tag{8}$$

It remains to express the thermal expectation value A via relation (4) as the parametric derivative of the extended

grand potential, taken while keeping μ, T and the shape of $V_{\text{ext}}(\mathbf{r})$ fixed. Crucially, instead of considering explicit many-body expressions, we adopt the classical density functional perspective [1–5] in order to find $A[\rho]$. We hence work with the grand potential in its density functional form: $\Omega[\rho] = F_{\text{id}}[\rho] + F_{\text{exc}}[\rho] + \int d\mathbf{r}\rho(\mathbf{r})[V_{\text{ext}}(\mathbf{r}) - \mu]$. Thereby the ideal gas free energy functional is $F_{\text{id}}[\rho] = k_B T \int d\mathbf{r}\rho(\mathbf{r})[\ln\rho(\mathbf{r}) - 1]$ and $F_{\text{exc}}[\rho]$ denotes the excess (over ideal gas) free energy functional.

Differentiating $\Omega[\rho]$ with respect to λ at fixed $V_{\text{ext}}(\mathbf{r})$ gives one direct contribution and one term arising from the induced changes in $\rho(\mathbf{r})$. The latter term, $\int d\mathbf{r}\delta\Omega[\rho]/\delta\rho(\mathbf{r})|_{V_{\text{ext}}}\partial\rho(\mathbf{r})/\partial\lambda$, vanishes due to the stationarity of the grand potential, $\delta\Omega[\rho]/\delta\rho(\mathbf{r})|_{V_{\text{ext}}} = 0$. The direct contribution is the derivative at fixed density, $-\partial\beta\Omega[\rho]/\partial\lambda|_\rho = -\partial\beta F_{\text{exc}}[\rho]/\partial\lambda|_\rho$, where we have exploited that the ideal, external, and chemical potential contributions to $\Omega[\rho]$ are independent of λ. From recalling Eq. (4), we obtain $A[\rho] = -\partial\beta F_{\text{exc}}[\rho]/\partial\lambda|_\rho$.

Functional calculus allows one to rewrite this formal expression for $A[\rho]$ as a functional integral [1,2,52]. Using the standard relation $c_1(\mathbf{r},[\rho]) = -\delta\beta F_{\text{exc}}[\rho]/\delta\rho(\mathbf{r})$ together with the definition (8) of the hyperdirect correlation functional $c_A(\mathbf{r},[\rho])$ gives

$$c_A(\mathbf{r},[\rho]) = \frac{\delta A[\rho]}{\delta\rho(\mathbf{r})}, \qquad (9)$$

$$A[\rho] = \int \mathcal{D}[\rho]c_A(\mathbf{r},[\rho]). \qquad (10)$$

The functional derivative (9) gives much further significance to the hyperdirect correlation functional $c_A(\mathbf{r},[\rho])$ as measuring changes of the thermal mean A against local perturbation of the density profile $\rho(\mathbf{r})$. Equation (10) is the inverse of Eq. (9) upon standard functional integration [1,2,52]. One can efficiently parametrize the functional integral, e.g., as $A[\rho] = \int d\mathbf{r}\rho(\mathbf{r})\int_0^1 da\, c_A(\mathbf{r},[a\rho])$, where the scaled density profile $a\rho(\mathbf{r})$ is obtained by multiplication of $\rho(\mathbf{r})$ with the parameter $0 \leq a \leq 1$. Equation (10) allows one to express the thermal average of a given observable as an explicit density functional $A[\rho]$, provided that the density functional dependence of $c_A(\mathbf{r},[\rho])$ is known.

As an initial test of this framework, we let the considered observable simply be the particle number $\hat{A}(\mathbf{r}^N) = N$, which we recall is a fluctuating variable in the grand ensemble. According to Eq. (3), we have $\chi_A(\mathbf{r}) = \text{cov}(\hat{\rho}(\mathbf{r}), N)$ and from Eq. (4) we obtain $N = -\partial\beta\Omega/\partial\lambda$. Furthermore Eq. (5) yields $\chi_A(\mathbf{r}) = \partial\rho(\mathbf{r})/\partial\lambda$. These are all key properties of the local compressibility $\chi_\mu(\mathbf{r}) = \beta\chi_A(\mathbf{r})$ [8,9,17–20] with the coupling parameter λ playing the role of the scaled chemical potential $\beta\mu$. Hence, for more

general observables $\hat{A}$, we conclude that $\chi_A(\mathbf{r})$ can be viewed as a corresponding generalization of $\chi_\mu(\mathbf{r})$.

We next address significantly more complex forms of $\hat{A}$. We therefore return to the hyper-Ornstein-Zernike equation (7) and consider the accessibility of the terms on its right-hand side on the basis of direct simulations and the methods provided by the recent neural functional theory [51,52]. Both the standard density profile $\rho(\mathbf{r})$ and the hyperfluctuation profile $\chi_A(\mathbf{r})$ can be sampled for given μ, T, and $V_{\text{ext}}(\mathbf{r})$, recall $\rho(\mathbf{r})$ as the average (1) and $\chi_A(\mathbf{r})$ as the covariance (3). For the given bare Hamiltonian H, the neural functional theory allows one to construct a neural-network-based representation of the direct correlation functional $c_1(\mathbf{r},[\rho])$ [51,52]. Automatic differentiation then straightforwardly provides a numerically efficient and accurate neural functional representation of $c_2(\mathbf{r},\mathbf{r}',[\rho])$ which is ready for use in Eq. (7). Evaluating the right-hand side of Eq. (7) then only requires the numerical integration over $\mathbf{r}'$.

Hence, for given μ, T, and $V_{\text{ext}}(\mathbf{r})$, the hyperdirect correlation function $c_A(\mathbf{r})$ that is specific for the considered inhomogeneous system can be computed explicitly via Eq. (7). This facilitates the generation of a training dataset from many-body simulation results. We do not invoke the functional dependence of $c_A(\mathbf{r},[\rho])$ for this task yet and require only standard grand canonical Monte Carlo simulation techniques [67–69] with no need to implement the extended ensemble explicitly.

Following the neural methodology for standard density functionals [51,52], this puts us in the position to machine learn the hyperfunctional map

$$\rho(\mathbf{r}') \rightarrow c_A(\mathbf{r}), \qquad (11)$$

where the density at positions $\mathbf{r}'$ removed from $\mathbf{r}$ will contribute with a range of nonlocality that is specific to the form of the observable $\hat{A}(\mathbf{r}^N)$. We proceed in analogy to Refs. [51,52] in constructing a neural network representation of $c_A(\mathbf{r},[\rho])$ via supervised machine learning on the basis of randomized training datasets, where at fixed temperature T, the value of μ and the shape of $V_{\text{ext}}(\mathbf{r})$ are varied. An illustration of the principal workflow is shown in Fig. 1 as applied to the following physical setup.

We first choose one-dimensional systems with either pure hard-core interactions or additional square-well attraction. We solely work on the basis of neural functionals to demonstrate the independence from the availability of analytic free energy functionals. We have checked that using Percus's exact free energy functional for hard rods [70,71] instead of its neural representation [52] generates no relevant numerical changes. The density profile under the influence of an external potential follows from numerical solution of the Euler-Lagrange equation (6) for $\lambda = 0$, using the respective neural one-body direct correlation functional. As an order parameter with genuine many-body
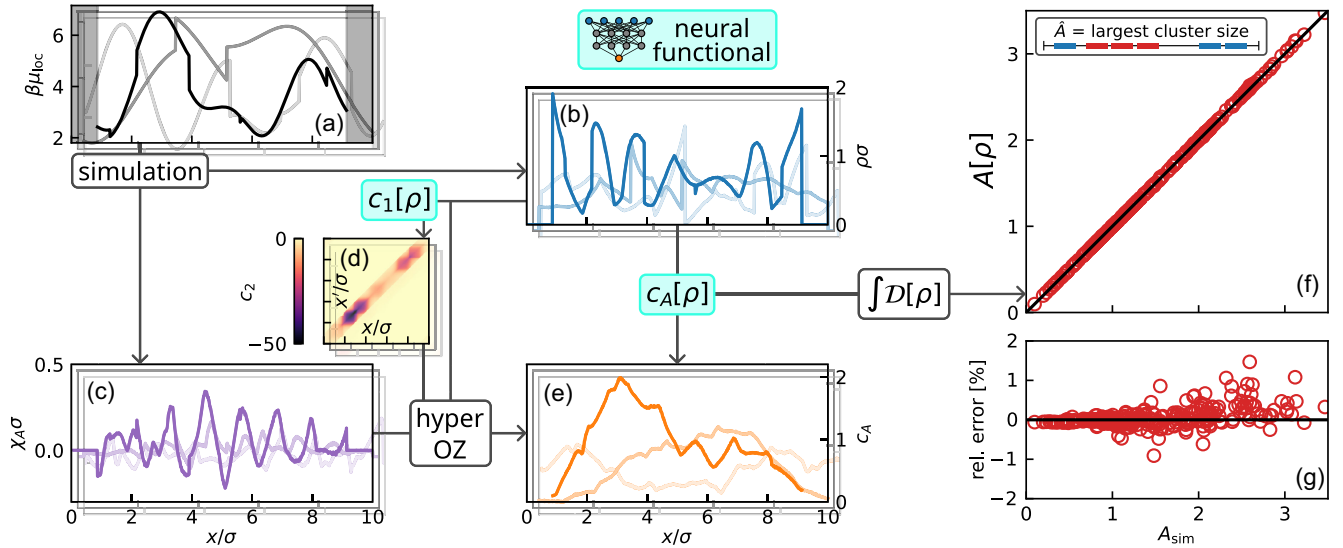
FIG. 1. Overview of hyperdensity functional theory. The observable $\hat{A}$ is chosen as the number of particles belonging to the largest cluster in hard rods of size σ. (a) A local chemical potential $\beta\mu_{\mathrm{loc}}(x) = \beta\mu - \beta V_{\mathrm{ext}}(x)$ creates spatially inhomogeneous systems. Shown are representative examples from 512 grand canonical Monte Carlo simulations with both randomized values of $\beta\mu$ and forms of $\beta V_{\mathrm{ext}}(x)$. (b) Corresponding scaled density profiles $\rho(x)\sigma$ sampled via Eq. (1). (c) Corresponding scaled hyperfluctuation profiles $\chi_A(x)\sigma$ obtained via Eq. (3). (d) Two-body direct correlation function $c_2(x, x', [\rho])$, as obtained via automatic differentiation from $c_1(x, [\rho])$ [51,52]. (e) Hyperdirect correlation functions $c_A(x)$ obtained by solving the hyper-Ornstein-Zernike equation (7). Using the density profile as input and the simulation results for $c_A(x)$ as target, supervised training yields a neural network that represents the hyperdirect correlation functional $c_A(x, [\rho])$. (f) Predicted values $A[\rho] = \int D[\rho] c_A(x, [\rho])$ from functional integration according to Eq. (10). For a test set of 256 systems not encountered during training, the predictions of $A[\rho]$ are compared against reference simulation data A_{sim}. (g) The relative numerical error of the predicted mean size A of the largest cluster is smaller than $\sim 1\%$.

character, we investigate cluster properties and therefore define two particles i and j as bonded if their positions x_i and x_j are within a bonding cutoff, $|x_i - x_j| < x_c$, where we choose $x_c = 1.2\sigma$, with the hard-core particle diameter σ. For each microstate of positions $x^N = x_1, \ldots, x_N$, we construct an instantaneous histogram that gives the number of clusters with (integer) size m, where a cluster consists of all particles that are bonded directly or mediated by other bonded particles. This is a standard criterion that is independent of dimensionality and used in studies of gelation [72,73].

Specifically, we choose $\hat{A}$ as the size of the largest cluster in a given microstate. We find studying and comparing the behavior of hard-core and square-well attractive rods to be a crucial test, as there is no way to assess the respective clustering properties via conventional density functional methods. Exemplary profiles are shown in Fig. 1 together with the numerical predictions from the neural functional $A[\rho]$, as evaluated via the functional integral (10). The neural predictions are highly accurate with a relative error consistently below $\sim 1\%$ as compared to the simulation reference.

On the basis of the availability of the neural hyperdirect correlation functional, we can formulate a template for stand-alone application of the hyperdensity functional theory to predict inhomogeneous states of a given fluid model, with no reliance on further simulation data. We

require trained neural network representations for $c_A(\mathbf{r}, [\rho])$ and $c_1(\mathbf{r}, [\rho])$. Automatic functional differentiation of the latter yields a neural representation of $c_2(\mathbf{r}, \mathbf{r}', [\rho])$.

First, in a conventional density functional setting the solution of the Euler-Lagrange equation (6) at given μ, T, and $V_{\mathrm{ext}}(\mathbf{r})$ yields the shape of the equilibrium density profile $\rho(\mathbf{r})$. This form is then used to evaluate the hyperdirect correlation functional $c_A(\mathbf{r}, [\rho])$ as well as $c_2(\mathbf{r}, \mathbf{r}', [\rho])$. The resulting functions turn the hyper-Ornstein-Zernike relation (7) into a concrete integral equation for determining the hyperfluctuation profile $\chi_A(\mathbf{r})$. Predictions for the mean value A in the considered system are obtained from calculating $A[\rho]$ at the known equilibrium density profile via numerical functional integration (10).

Figure 2 shows results from this strategy applied to the cluster statistics of both the hard rod and square-well system (potential range 0.2σ and depth $\beta\epsilon = 1$) [74]. We consider confinement between two hard walls, but with no further disturbing influence as was present during training. This clean situation tests the genuine extrapolation capability of the neural functionals. The results shown in Fig. 2 achieve excellent agreement with reference simulation data. This successful application demonstrates that we have developed a systematic functional approach that allows one to address the equilibrium behavior of general observables. The statistical mechanical many-body problem is thereby cast into functional form, which we have shown to
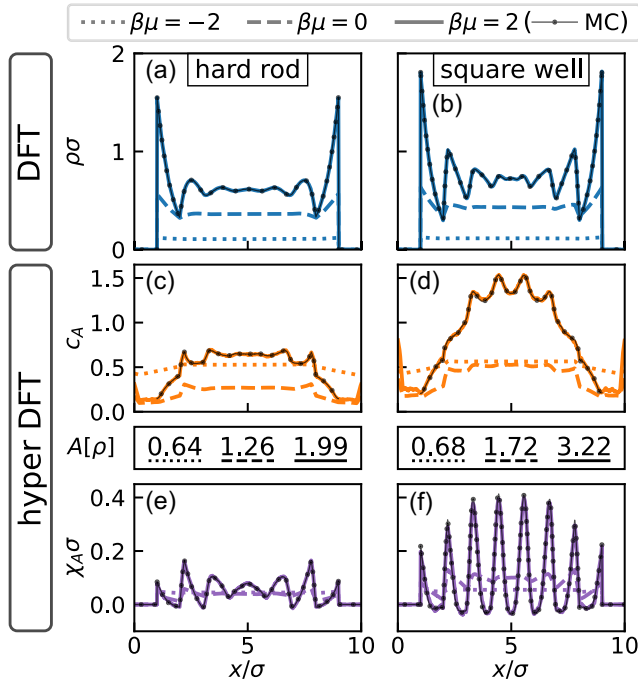
FIG. 2. Application of the hyperdensity functional theory to the statistics of the largest cluster of hard rods (a),(c),(e) and attractive square-well rods (b),(d),(f). The systems are confined between two hard walls with separation distance $L = 8\sigma$ and the profiles are shown as a function of the scaled distance x/σ across the pore for $\beta\mu = -2$ (dotted), 0 (dashed), and 2 (solid lines). We depict theoretical results for the density profile $\rho(x)\sigma$ (a),(b), the hyperdirect correlation function $c_A(x)$ (c),(d), the mean value $A[\rho]$, and the hyperfluctuation profile $\chi_A(x)\sigma$ (e),(f). For the case of largest chemical potential, Monte Carlo simulation results are shown as reference (solid lines with symbols). These coincide with the respective theoretical predictions on the scale of the plot. The simulated reference values for A are identical within the quoted accuracy to the neural predictions $A[\rho]$.

be accessible via simulation-based training of neural networks that can be applied efficiently in predictive tasks.

We demonstrate that the demands for training the neural functionals $c_1(\mathbf{r}, [\rho])$ and $c_A(\mathbf{r}, [\rho])$ are not prohibitive for studying complex order parameters in realistic fluid models by successful application of the cluster analysis to the hard sphere system in three dimensions, as shown in Supplemental Material [75]. As all quantities in the framework have physical interpretations, with $\chi_A(\mathbf{r})$ generalizing the prominently used local compressibility $\chi_\mu(\mathbf{r})$ [8,9,17–20] and thermal susceptibility $\chi_T(\mathbf{r})$ [18–20], it seems feasible that existing density functional methods [1–4] could be applied in analytical hyperfunctional construction. The ease with which neural hyperfunctionals can be trained can motivate such work. Analytical treatments of simple one- and two-body forms of $\hat{A}(\mathbf{r}^N)$, the relationships to a static version of the countoscope [76] and to force-density functional theory [77], along with a description of the role of $\chi_A(\mathbf{r})$ as the local compressibility and in the hyperforce

theory [35] are given in Supplemental Material [75]. While we have focused on dependence on position, we see no formal problems in incorporating orientational degrees of freedom. The increase in complexity could be alleviated by the use of molecular density functional methods [11–13]. Investigating deeper relationships with functional thermo-dynamics [65], thermal Noether invariance [33–35], and power functional theory [5] is worthwhile.

Data availability—Source code, simulation data, and neural functionals are available at [74].

[1] R. Evans, The nature of the liquid-vapour interface and other topics in the statistical mechanics of non-uniform, classical fluids, Adv. Phys. **28**, 143 (1979).

[2] R. Evans, Density functionals in the theory of nonuniform fluids, Chap. 3 in *Fundamentals of Inhomogeneous Fluids*, edited by D. Henderson (Dekker, New York, 1992).

[3] R. Evans, M. Oettel, R. Roth, and G. Kahl, New developments in classical density functional theory, J. Phys. Condens. Matter **28**, 240401 (2016).

[4] J. P. Hansen and I. R. McDonald, *Theory of Simple Liquids*, 4th ed. (Academic Press, London, 2013).

[5] M. Schmidt, Power functional theory for many-body dynamics, Rev. Mod. Phys. **94**, 015007 (2022).

[6] R. Evans, D. Frenkel, and M. Dijkstra, From simple liquids to colloids and soft matter, Phys. Today **72**, No. 2, 38 (2019).

[7] M. Levesque, R. Vuilleumier, and D. Borgis, Scalar fundamental measure theory for hard spheres in three dimensions: Application to hydrophobic solvation, J. Chem. Phys. **137**, 034115 (2012).

[8] R. Evans and M. C. Stewart, The local compressibility of liquids near non-adsorbing substrates: A useful measure of solvophobicity and hydrophobicity?, J. Phys. Condens. Matter **27**, 194111 (2015).

[9] R. Evans, M. C. Stewart, and N. B. Wilding, A unified description of hydrophilic and superhydrophobic surfaces in terms of the wetting and drying transitions of liquids, Proc. Natl. Acad. Sci. U.S.A. **116**, 23901 (2019).

[10] M. K. Coe, R. Evans, and N. B. Wilding, Density depletion and enhanced fluctuations in water near hydrophobic solutes: Identifying the underlying physics, Phys. Rev. Lett. **128**, 045501 (2022).

[11] G. Jeanmairet, M. Levesque, and D. Borgis, Molecular density functional theory of water describing hydrophobicity at short and long length scales, J. Chem. Phys. **139**, 154101 (2013).

[12] G. Jeanmairet, M. Levesque, R. Vuilleumier, and D. Borgis, Molecular density functional theory of water, J. Phys. Chem. Lett. **4**, 619 (2013).

[13] S. Luukkonen, M. Levesque, L. Belloni, and D. Borgis, Hydration free energies and solvation structures with molecular density functional theory in the hypernetted chain approximation, J. Chem. Phys. **152**, 064110 (2020).

[14] D. Martin-Jimenez, E. Chacón, P. Tarazona, and R. Garcia, Atomically resolved three-dimensional structures of electrolyte aqueous solutions near a solid surface, Nat. Commun. **7,** 12164 (2016).

[15] J. Hernández-Muñoz, E. Chacón, and P. Tarazona, Density functional analysis of atomic force microscopy in a dense fluid, J. Chem. Phys. **151,** 034701 (2019).

[16] P. Cats, R. Evans, A. Härtel, and R. van Roij, Primitive model electrolytes in the near and far field: Decay lengths from DFT and simulations, J. Chem. Phys. **154,** 124504 (2021).

[17] N. B. Wilding, R. Evans, and F. Turci, What is the best simulation approach for measuring local density fluctuations near solvo/hydrophobes?, J. Chem. Phys. **160,** 164103 (2024).

[18] T. Eckert, N. C. X. Stuhlmüller, F. Sammüller, and M. Schmidt, Fluctuation profiles in inhomogeneous fluids, Phys. Rev. Lett. **125,** 268004 (2020).

[19] T. Eckert, N. C. X. Stuhlmüller, F. Sammüller, and M. Schmidt, Local measures of fluctuations in inhomogeneous liquids: Statistical mechanics and illustrative applications, J. Phys. Condens. Matter **35,** 425102 (2023).

[20] M. K. Coe, R. Evans, and N. B. Wilding, Understanding the physics of hydrophobic solvation, J. Chem. Phys. **158,** 034508 (2023).

[21] Z. Zhang and W. Kob, Revealing the three-dimensional structure of liquids using four-point correlation functions, Proc. Natl. Acad. Sci. U.S.A. **117,** 14032 (2020).

[22] N. Singh, Z. Zhang, A. K. Sood, W. Kob, and R. Ganapathy, Intermediate-range order governs dynamics in dense colloidal liquids, Proc. Natl. Acad. Sci. U.S.A. **120,** e2300923120 (2023).

[23] I. Pihlajamaa, C. C. L. Laudicina, C. Luo, and L. M. C. Janssen, Emergent structural correlations in dense liquids, PNAS Nexus **2,** pgad184 (2023).

[24] R. Evans and A. O. Parry, Liquids at interfaces: What can a theorist contribute?, J. Phys. Condens. Matter **2,** SA15 (1990).

[25] J. R. Henderson, Statistical mechanical sum rules, Chap. 2 in *Fundamentals of Inhomogeneous Fluids*, edited by D. Henderson (Dekker, New York, 1992).

[26] M. Revzen, Functional integrals in statistical physics, Am. J. Phys. **38,** 611 (1970).

[27] I. Marvian and R. W. Spekkens, Extending Noether's theorem by quantifying the asymmetry of quantum states, Nat. Commun. **5,** 3821 (2014).

[28] S. I. Sasa and Y. Yokokura, Thermodynamic entropy as a Noether invariant, Phys. Rev. Lett. **116,** 140601 (2016).

[29] S. Sasa, S. Sugiura, and Y. Yokokura, Thermodynamical path integral and emergent symmetry, Phys. Rev. E **99,** 022109 (2019).

[30] Y. A. Budkov and A. L. Kolesnikov, Modified Poisson-Boltzmann equations and macroscopic forces in inhomogeneous ionic fluids, J. Stat. Mech. (2022) 053205.

[31] P. E. Brandyshev and Y. A. Budkov, Noether's second theorem and covariant field theory of mechanical stresses in inhomogeneous ionic fluids, J. Chem. Phys. **158,** 174114 (2023).

[32] A. Bravetti, M. A. Garcia-Ariza, and D. Tapias, Thermodynamic entropy as a Noether invariant from contact geometry, Entropy **25,** 1082 (2023).

[33] S. Hermann and M. Schmidt, Noether's theorem in statistical mechanics, Commun. Phys. **4,** 176 (2021).

[34] S. Hermann and M. Schmidt, Why Noether's theorem applies to statistical mechanics, J. Phys. Condens. Matter **34,** 213001 (2022) (Topical Review).

[35] S. Robitschko, F. Sammüller, M. Schmidt, and S. Hermann, Hyperforce balance from thermal Noether invariance of any observable, Commun. Phys. **7,** 103 (2024).

[36] J. O. Hirschfelder, Classical and quantum mechanical hypervirial theorems, J. Chem. Phys. **33,** 1462 (1960).

[37] P. S. Clegg, Characterising soft matter using machine learning, Soft Matter **17,** 3991 (2021).

[38] M. Dijkstra and E. Luijten, From predictive modelling to machine learning and reverse engineering of colloidal self-assembly, Nat. Mater. **20,** 762 (2021).

[39] E. Boattini, M. Dijkstra, and L. Filion, Unsupervised learning for local structure detection in colloidal systems, J. Chem. Phys. **151,** 154901 (2019).

[40] G. Campos-Villalobos, E. Boattini, L. Filion, and M. Dijkstra, Machine learning many-body potentials for colloidal systems, J. Chem. Phys. **155,** 174902 (2021).

[41] G. Campos-Villalobos, G. Giunta, S. Marín-Aguilar, and M. Dijkstra, Machine-learning effective many-body potentials for anisotropic particles using orientation-dependent symmetry functions, J. Chem. Phys. **157,** 024902 (2022).

[42] T. Santos-Silva, P. I. C. Teixeira, C. Anquetil-Deck, and D. J. Cleaver, Neural-network approach to modeling liquid crystals in complex confinement, Phys. Rev. E **89,** 053316 (2014).

[43] S.-C. Lin and M. Oettel, A classical density functional from machine learning and a convolutional neural network, SciPost Phys. **6,** 025 (2019).

[44] S.-C. Lin, G. Martius, and M. Oettel, Analytical classical density functionals from an equation learning network, J. Chem. Phys. **152,** 021102 (2020).

[45] P. Cats, S. Kuipers, S. de Wind, R. van Damme, G. M. Coli, M. Dijkstra, and R. van Roij, Machine-learning free-energy functionals using density profiles from simulations, APL Mater. **9,** 031109 (2021).

[46] C. Qiao, X. Yu, X. Song, T. Zhao, X. Xu, S. Zhao, and K. E. Gubbins, Enhancing gas solubility in nanopores: A combined study using classical density functional theory and machine learning, Langmuir **36,** 8527 (2020).

[47] P. Yatsyshin, S. Kalliadasis, and A. B. Duncan, Physics-constrained Bayesian inference of state functions in classical density-functional theory, J. Chem. Phys. **156,** 074105 (2022).

[48] A. Malpica-Morales, P. Yatsyshin, M. A. Duran-Olivencia, and S. Kalliadasis, Physics-informed Bayesian inference of external potentials in classical density functional theory, J. Chem. Phys. **159,** 104109 (2023).

[49] X. Fang, M. Gu, and J. Wu, Reliable emulation of complex functionals by active learning with error control, J. Chem. Phys. **157,** 214109 (2022).

[50] D. de las Heras, T. Zimmermann, F. Sammüller, S. Hermann, and M. Schmidt, Perspective: How to overcome

dynamical density functional theory, J. Phys. Condens. Matter **35**, 271501 (2023). (Invited Perspective).

[51] F. Sammüller, S. Hermann, D. de las Heras, and M. Schmidt, Neural functional theory for inhomogeneous fluids: Fundamentals and applications, Proc. Natl. Acad. Sci. U.S.A. **120**, e2312484120 (2023).

[52] F. Sammüller, S. Hermann, and M. Schmidt, Why neural functionals suit statistical mechanics, J. Phys. Condens. Matter **36**, 243002 (2024) (Invited Topical Review).

[53] J. Dijkman, M. Dijkstra, R. van Roij, M. Welling, J.-W. van de Meent, and B. Ensing, Learning neural free-energy functionals with pair-correlation matching, arXiv:2403.15007.

[54] F. Sammüller and M. Schmidt, Neural density functionals: Local learning and pair correlation matching, arXiv:2406.03327 [Phys. Rev. E (to be published)].

[55] M. M. Kelley, J. Quinton, K. Fazel, N. Karimitari, C. Sutton, and R. Sundararaman, Bridging electronic and classical density-functional theory using universal machine-learned functional approximations, arXiv:2405.20270.

[56] R. Nagai, R. Akashi, S. Sasaki, and S. Tsuneyuki, Neural-network Kohn-Sham exchange-correlation potential and its out-of-training transferability, J. Chem. Phys. **148**, 241737 (2018).

[57] J. Schmidt, C. L. Benavides-Riveros, and M. A. L. Marques, Machine learning the physical nonlocal exchange-correlation functional of density-functional theory, J. Phys. Chem. Lett. **10**, 6425 (2019).

[58] Y. Zhou, J. Wu, S. Chen, and G. Chen, Toward the exact exchange-correlation potential: A three-dimensional convolutional neural network construct, J. Phys. Chem. Lett. **10**, 7264 (2019).

[59] R. Nagai, R. Akashi, and O. Sugino, Completing density functional theory by machine learning hidden messages from molecules, npj Comput. Mater. **6**, 43 (2020).

[60] L. Li, S. Hoyer, R. Pederson, R. Sun, E. D. Cubuk, P. Riley, and K. Burke, Kohn-Sham equations as regularizer: Building prior knowledge into machine-learned physics, Phys. Rev. Lett. **126**, 036401 (2021).

[61] H. Li, N. Zou, M. Ye, R. Xu, X. Gong, and W. Duan, Deep-learning density functional theory Hamiltonian for efficient *ab initio* electronic-structure calculation, Nat. Comput. Sci. **2**, 367 (2022).

[62] J. Gedeon, J. Schmidt, M. J. P. Hodgson, J. Wetherell, C. L. Benavides-Riveros, and M. A. L. Marques, Machine learning the derivative discontinuity of density-functional theory, Mach. Learn.: Sci. Technol. **3**, 015011 (2022).

[63] R. Pederson, B. Kalita, and K. Burke, Machine learning and density functional theory, Nat. Rev. Phys. **4**, 357 (2022).

[64] R. Zwanzig, *Nonequilibrium Statistical Mechanics* (Oxford University Press, Oxford, 2001).

[65] J. G. Anero, P. Español, and P. Tarazona, Functional thermodynamics: A generalization of dynamic density functional theory to non-isothermal situations, J. Chem. Phys. **139**, 034106 (2013).

[66] N. D. Mermin, Thermal properties of the inhomogeneous electron gas, Phys. Rev. **137**, A1441 (1965).

[67] D. Frenkel and B. Smit, *Understanding Molecular Simulation: From Algorithms to Applications*, 3rd ed. (Academic Press, London, 2023).

[68] N. B. Wilding, Computer simulation of fluid phase transitions, Am. J. Phys. **69**, 1147 (2001).

[69] A. V. Brukhno, J. Grant, T. L. Underwood, K. Stratford, S. C. Parker, J. A. Purton, and N. B. Wilding, DL_MONTE: A multipurpose code for Monte Carlo simulation, Mol. Simul. **47**, 131 (2021).

[70] J. K. Percus, Equilibrium state of a classical fluid of hard rods in an external field, J. Stat. Phys. **15**, 505 (1976).

[71] A. Robledo and C. Varea, On the relationship between the density functional formalism and the potential distribution theory for nonuniform fluids, J. Stat. Phys. **26**, 513 (1981).

[72] R. B. Jadrich, D. J. Milliron, and T. M. Truskett, Colloidal gels, J. Chem. Phys. **159**, 090401 (2023).

[73] F. Sammüller, D. de las Heras, and M. Schmidt, Inhomogeneous steady shear dynamics of a three-body colloidal gel former, J. Chem. Phys. **158**, 054908 (2023). (Special Topic on Colloidal Gels).

[74] F. Sammüller, S. Robitschko, S. Hermann, M. Schmidt, Hyperdensity functional theory of soft matter (2024), 10.5281/zenodo.13318634.

[75] See Supplemental Material at http://link.aps.org/supplemental/10.1103/PhysRevLett.133.098201 for simulation results for the 3D hard sphere fluid, additional information about the treatment of simple observables, and the connection to the hyperforce theory.

[76] E. K. R. Mackay, S. Marbach, B. Sprinkle, and A. L. Thorneywork, The countoscope: Measuring self and collective dynamics without trajectories, arXiv:2311.00647.

[77] S. M. Tschopp, F. Sammüller, S. Hermann, M. Schmidt, and J. M. Brader, Force density functional theory in- and out-of-equilibrium, Phys. Rev. E **106**, 014115 (2022).